Role of baryonic resonances in the dilepton emission in nucleon-nucleon collisions

R. Shyam* and U. Mosel
Institut für Theoretische Physik, Universität Giessen, D-35392 Giessen, Germany
(Received 5 March 2003; published 20 June 2003)

Within an effective Lagrangian model, we present calculations for cross sections of the dilepton production in proton-proton and proton-neutron collisions at laboratory kinetic energies in 1–5 GeV range. Production amplitudes include contributions from the nucleon-nucleon bremsstrahlung as well as from the mechanism of excitation, propagation, and radiative decay of $\Delta(1232)$ and $N^*(1520)$ intermediate baryonic resonances. It is found that the delta isobar terms dominate the cross sections in the entire considered beam energy range. Our calculations are able to explain the data of the DLS Collaboration on the dilepton production in proton-proton collisions for beam energies below 1.3 GeV. However, for incident energies higher than this the inclusion of contributions from other dilepton sources such as Dalitz decay of π^0 and η mesons, and direct decay of ρ^0 and ω mesons is necessary to describe the data.

DOI: 10.1103/PhysRevC.67.065202 PACS number(s): 25.75.Dw, 13.30.Ce, 12.40.Yx

I. INTRODUCTION

Dileptons observed in the nucleus-nucleus collisions travel relatively unscathed from the production point to the detector. Therefore, they are expected to provide clear information about the early dense and hot stage of heavy ion collisions [1–3], which is in contrast to the hadronic probes which often suffer from strong final state interactions and the information about the collision history carried by them may be lost due to the rescattering in the expansion phase [4]. One of the phenomena predicted [5–13] at higher nuclear matter densities is the restoration of chiral symmetry that is manifested in the modification of masses of the vector mesons as a function of the nuclear matter density. Consequences of this effect can be observed in the dilepton (e^+e^-) spectra measured in nucleus-nucleus collisions [14]. Enhancements (above known sources) observed in the measured [15,16] soft lepton pair production cross sections in heavy ion collisions at the SPS energies, have been attributed [17–21] to in-medium modifications of the vector meson properties rather than to reflection of a new state of hadronic matter. However, such a scenario has not been fully successful [22–24] in explaining the dilepton spectra measured in these reactions at much lower beam energies (a few GeV/nucleon) [25] where the temperature and density regime are different and one does not expect a phase transition.

In this context, the investigation of the dilepton production in elementary nucleon-nucleon (NN) collisions is of interest because the corresponding cross sections enter into the transport model calculations of the e^+e^- spectra in the heavy ion collisions. Therefore, a quantitative understanding of this process is a natural prerequisite to an unequivocal determination of in-medium effects mentioned above. The study of this process is of interest in its own right [26] as it is expected to provide deeper insight into the hadronic structure and the photon-hadron interactions. This investigation may give fundamental information on the electromagnetic form factor of the nucleon in the timelike region around the vector-meson masses, which is otherwise hard to access (see, e.g., Ref. [4]).

It has been known for some time that intermediate baryonic resonances play an important role in the dilepton production in the NN collisions. Dalitz decay of the Δ isobar has been shown to be a strong dilepton production channel [27–29]. The importance of the baryonic resonance $N^*(1520)$ has been emphasized for this process in Refs. [30,31] where it is pointed out that the subthreshold ρ production (and its subsequent decay) via this resonance makes important contributions to the dilepton spectrum observed in the proton-proton (pp) collisions. Therefore, the investigation of the dilepton production is expected to provide a useful tool to probe the parameters (e.g., coupling constants, form factors, etc.) of the nucleon-resonance-photon vertices and masses and widths of the relevant nucleon resonances.

The aim of this paper is to investigate the dilepton production in nucleon-nucleon collisions in the beam energy range of 1–5 GeV within an effective Lagrangian model (ELM), which has been successfully applied to the description of pion and associated kaon production in pp collisions [32–34]. Initial interaction between two incoming nucleons is modeled by an effective Lagrangian which is based on the exchange of the π, ρ, ω, and σ mesons. The coupling constants at the nucleon-nucleon-meson vertices are determined by directly fitting the T matrices of the NN scattering in the relevant energy region. The effective Lagrangian uses the pseudovector (PV) coupling for the nucleon-nucleon-pion vertex and thus incorporates the low energy theorems of current algebra and the hypothesis of partially conserved axial current (PCAC). The e^+e^- production proceeds via excitation, propagation and radiative decay of $\Delta(1232)$ and $N^*(1520)$ baryonic resonance states. Also included are the nucleon intermediate states (which gives rise to the NN bremsstrahlung contribution). The interference terms between various amplitudes are taken into account. The gauge invariance at the electromagnetic vertices is preserved in our calculations. Our model is similar in spirit to those of Refs. [29,35,36]. However, in Ref. [36] no resonance contribution was considered whereas in Refs. [29,35] resonance contributions were limited to the Δ isobar only. The latter, though,

*On leave from Saha Institute of Nuclear Physics, Calcutta, India.

did include the interference between the nucleon and Δ terms. In calculations presented in Refs. [30,31,37], NN bremsstrahlung contributions were ignored. We would like to stress that in Refs. [30,31] constant matrix elements have been used for various processes and the total dilepton production cross sections have been calculated by adding the corresponding cross sections and not the amplitudes, so part of the motivation of the present study is the investigation of the so far neglected quantum mechanical effects.

We investigate the role of baryonic resonances in the invariant mass spectrum of the dilepton produced in proton-proton and proton-neutron collisions at various beam energies in the 1–5 GeV range. To this end, we present the first field theoretic calculation of the dilepton production in NN collisions where excitation, propagation, and radiative decay of the $N^*(1520)$ baryonic resonance are fully accounted for. We also compare our calculations with the published data [38] on the dilepton production in elementary proton-proton collisions, by the Dilepton spectrometer (DLS) collaboration. In order to describe these data the contributions from other dilepton sources (π^0 and η Dalitz decay and direct decay of ρ^0 and ω mesons) have also been considered.

The remainder of this paper is organized in the following way. Section II contains details of our theoretical approach. Section III comprises the results of our analysis and their discussions. The summary and conclusions of our work are presented in Sec. IV.

II. FORMALISM

A representative of the lowest order Feynman diagrams contributing to the dilepton production, as considered by us, is shown in Fig. 1. The intermediate nucleon or resonances can radiate a virtual photon that decays into a dilepton [Figs. 1(a) and 1(b)]. There are also their exchange counterparts. In addition, there are diagrams of these types where the virtual photon is emitted from the nucleon line on the right side. The internal meson lines can also lead to dilepton emission [see Fig. 1(c)]. Momenta of various particles are indicated in Fig. 1(a). q, p_i, and k are four momenta of the exchanged meson, the intermediate resonance (or nucleon), and the photon, respectively. To evaluate various amplitudes, we have used the effective Lagrangians for the nucleon-nucleon-meson, resonance-nucleon-meson, nucleon-nucleon-photon, and resonance-nucleon-photon vertices. These are discussed in the following sections.

A. Nucleon-nucleon-meson vertex

As done before in the investigation of $pp \to pp\pi^0$, $pp \to pn\pi^+$ [32], and $pp \to p\Lambda K^+$ [34] reactions, the parameters for these vertices are determined by fitting the NN elastic scattering T matrix with an effective NN interaction based on the π, ρ, ω, and σ meson exchanges. The effective meson-NN Lagrangians are (see, e.g., Refs. [39,40])

$$\mathcal{L}_{NN\pi} = -\frac{g_{NN\pi}}{2m_N}\bar{\Psi}_N \gamma_5 \gamma_\mu \boldsymbol{\tau}\cdot(\partial^\mu \boldsymbol{\Phi}_\pi)\Psi_N, \tag{1}$$

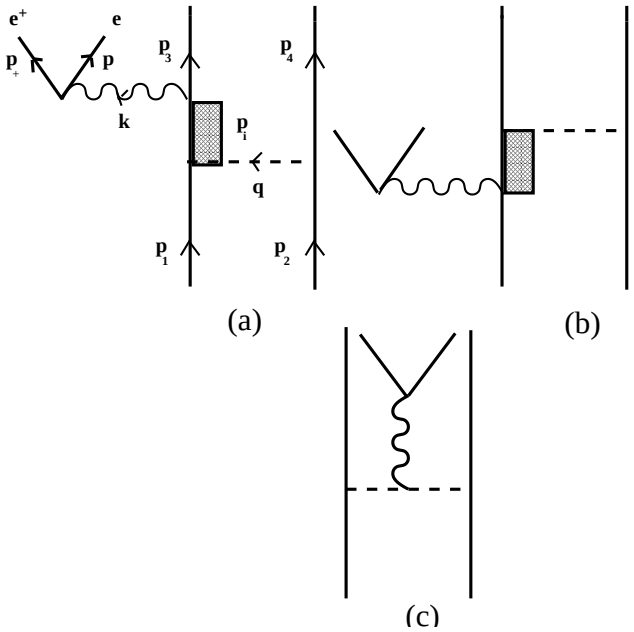

FIG. 1. A representative of Feynman diagrams for emission of dilepton in nucleon-nucleon collisions as considered in this work. (a) denotes emission after NN collisions, (b) before NN collision, and (c) during NN collision. The box represents any of an off-shell nucleon, a Δ isobar, or a N^* resonance.

$$\mathcal{L}_{NN\rho} = -g_{NN\rho}\bar{\Psi}_N\left(\gamma_\mu + \frac{k_\rho}{2m_N}\sigma_{\mu\nu}\partial^\nu\right)\boldsymbol{\tau}\cdot\boldsymbol{\rho}^\mu\Psi_N, \tag{2}$$

$$\mathcal{L}_{NN\omega} = -g_{NN\omega}\bar{\Psi}_N\left(\gamma_\mu + \frac{k_\omega}{2m_N}\sigma_{\mu\nu}\partial^\nu\right)\omega^\mu\Psi_N, \tag{3}$$

$$\mathcal{L}_{NN\sigma} = g_{NN\sigma}\bar{\Psi}_N\sigma\Psi_N. \tag{4}$$

In Eqs. (1)–(4), we have used the notations and conventions of Bjorken and Drell [41] and definitions of various terms are the same as those given there. In Eq. (1) m_N denotes the nucleon mass. It should be noted that we use a PV coupling for the $NN\pi$ vertex. Since these Lagrangians are used to directly model the NN T matrix, we have also included a nucleon-nucleon-axial-vector-isovector vertex, with the effective Lagrangian given by

$$\mathcal{L}_{NNA} = g_{NNA}\bar{\Psi}\gamma_5\gamma_\mu\boldsymbol{\tau}\Psi\cdot\mathbf{A}^\mu, \tag{5}$$

where **A** represents the axial-vector meson field. This term is introduced because if the mass of the axial meson A is chosen to be very large ($\gg m_N$) [29] and g_{NNA} is defined as

$$g_{NNA} = \frac{1}{\sqrt{3}}m_A\left(\frac{g_{NN\pi}}{2m_N}\right), \tag{6}$$

it cures the unphysical behavior in the angular distribution of NN scattering caused by the contact term in the one-pion exchange amplitude. It should be mentioned here that A is different from the $a_1(1260)$ meson resonance to be discussed later on. The role of the A vertex is to explicitly subtract out

TABLE I. Coupling constants for the *NN*-meson vertices used in the calculations.

Meson	$g^2/4\pi$	ℓ	Λ (GeV)	Mass (GeV)
π	12.562	0.1133	1.005	0.138
σ	2.340	0.1070	1.952	0.550
ω	46.035	0.0985	0.984	0.783
ρ	0.317	0.1800	1.607	0.770
$k_\rho = 6.033,\ k_\omega = 0.0$				

the contact term of the one-pion exchange part of the *NN* interaction. A similar term in the coordinate space potential is effectively switched off by the repulsive hard core.

At each interaction vertex, the following form factor is introduced:

$$F_i^{NN} = \left(\frac{\lambda_i^2 - m_i^2}{\lambda_i^2 - q_i^2} \right), \quad i = \pi, \rho, \sigma, \omega, \tag{7}$$

where q_i and m_i are the four momentum and mass of the ith exchanged meson and λ_i is the corresponding cutoff parameter. The latter governs the range of suppression of the contributions of high momenta, which is done via the form factor. Since *NN* scattering cross sections decrease gradually with the beam energy (beyond a certain value) and since we fit the elastic *T* matrix directly, the coupling constants are expected to be energy dependent. Therefore, while keeping the cutoffs λ_i [in Eq. (7)] energy independent, we take energy dependent meson-nucleon coupling constants of the following form:

$$g(\sqrt{s}) = g_0 \exp(-\ell \sqrt{s}), \tag{8}$$

where *s* is the square of the total c.m. energy. The parameters g_0, ℓ, and λ have been determined by fitting the *T* matrix to the relevant proton-proton and proton-neutron scattering data at beam energies in the range of 800 MeV–4.00 GeV [29]. Signs of the effective Lagrangians [Eqs. (1)–(5)] are also fixed by this procedure. The values of various parameters are given in Table I [signs of all the coupling constants (g) are positive]. In this table the parameters of the *A* exchange vertex are not explicitly shown as they are related to those of the pion via Eq. (6). The mass of the *A* meson is taken to be 18 GeV. The same parameters have also been used to describe the initial *NN* interaction in calculations reported in Refs. [29,32,34]. This ensures that the *NN* elastic scattering channel remains the same in the description of various inelastic processes within this model, as it should be.

The exchange of the a_1 meson (mass being 1260 MeV), which is the chiral partner of the ρ meson, has also been considered by some authors [42] in the description of the *NN* interaction. However, its contribution is masked to a considerable extent by the strong short-ranged repulsion originating from ω exchange. Moreover, as can be seen from Table I, values of the cutoff parameters appearing in the form factors [Eq. (7)] are in the region of 1.0–2.0 GeV. It does not seem meaningful to include exchange of mesons with masses lying in the region where modifications due to the extended structure of hadrons are applied. Nevertheless, the a_1 meson (if included) can contribute to the dilepton spectrum through diagrams such as that shown in Fig. 1(c). However, the couplings of this meson to nucleons and resonances are largely unknown. In any case, contributions of such processes are expected to be of relevance only for the dilepton invariant masses greater than 1.5 GeV [43]. This region is excluded by the DLS data. Due to these reasons we have not included the exchange of the a_1 meson in our calculations.

B. Resonance-nucleon-meson vertex

In addition to nucleonic intermediate states (*NN* bremsstrahlung), we have considered in this work also the contributions from the $\Delta(1232)$ isobar and $N^*(1520)$ nucleon resonance intermediate states. The latter is a spin-$\frac{3}{2}$ negative parity resonance. While only π and ρ mesons couple to Δ isobar, all of the four exchanged mesons, namely, π, ρ, ω, and σ can couple to $N^*(1520)$ resonance.

For spin-$\frac{3}{2}$ resonances, we use the following effective Lagrangians [44]:

$$\mathcal{L}_{RN\pi} = \frac{g_{RN\pi}}{m_\pi} \bar{\Psi}_\mu^R \Gamma_\pi \partial^\mu \mathbf{\Phi}_\pi \Psi_N + \text{H.c.}, \tag{9}$$

$$\mathcal{L}_{RN\rho} = i \frac{g_{RN\rho}}{m_\rho} \bar{\Psi}_\mu^R (\partial^\nu \boldsymbol{\rho}^\mu - \partial^\mu \boldsymbol{\rho}^\nu) \gamma_\nu \Gamma \Psi_N + \text{H.c.}, \tag{10}$$

$$\mathcal{L}_{RN\omega} = i \frac{g_{RN\omega}}{m_\omega} \bar{\Psi}_\mu^R (\partial^\nu \omega^\mu - \partial^\mu \omega^\nu) \gamma_\nu \Gamma \Psi_N + \text{H.c.}, \tag{11}$$

$$\mathcal{L}_{RN\sigma} = \frac{g_{RN\sigma}}{m_\sigma} \bar{\Psi}_\mu^R \Gamma_\pi (\partial^\mu \sigma) \Psi_N + \text{H.c.}, \tag{12}$$

Here, $\bar{\Psi}_\mu^R$ is the vector spinor for the spin-$\frac{3}{2}$ particle. In Eqs. [(8)–(11)], the operator Γ_π is unity for even parity resonance and γ_5 for the odd parity one, whereas Γ is γ_5 for the even parity resonance and unity for the odd parity one. The meson fields in the above equations need to be replaced by $\boldsymbol{\tau} \cdot \phi$ (where ϕ corresponds to π, ρ, ω, or σ meson fields) and $\mathbf{T} \cdot \phi$ (where $\mathbf{T}$ and $\boldsymbol{\tau}$ are the isospin transition operator and Pauli isospin matrices, respectively) for isospin-$\frac{1}{2}$ and isospin-$\frac{3}{2}$ resonances, respectively.

The values of the coupling constants $g_{\Delta N\pi}$ and $g_{\Delta N\rho}$ are shown in Table II; these are the same as those determined in Ref. [29] by fitting to experimental data on $pp \to n\Delta^{++}$ reaction at kinetic energies in the range of 1–2 GeV. We have assumed that the off-shell dependence of the resonance-nucleon vertex is determined solely by multiplying the vertex constant by a form factor. Similar to Refs. [29,32], we have used the following form factor for the Δ vertices:

$$F_i^{N\Delta} = \left[\frac{(\lambda_i^\Delta)^2 - m_i^2}{(\lambda_i^\Delta)^2 - q_i^2} \right]^2, \quad i = \pi, \rho, \tag{13}$$

TABLE II. Coupling constants and cutoff parameters for the resonance-nucleon-meson vertices used in the calculations.

Resonance	Decay channel	g	Cutoff parameter (GeV)
$\Delta(1232)$	$N\pi$	2.13	1.421
	$N\rho$	7.14	2.273
$N^*(1520)$	$N\pi$	1.55	0.800
	$N\rho$	6.44	0.800
	$N\omega$	3.42	0.800
	$N\sigma$	1.24	0.800

with the values of the cutoff parameters as λ_π^Δ and λ_ρ^Δ as given in Table II, which are exactly the same as those used earlier [29,32,34].

For the $N^*N\pi$ and $N^*N\rho$ vertices the coupling constants have been determined from the observed branching ratios for the decay of the resonance to $N\pi$ and $N\rho$ channels, respectively. In the later case the finite lifetime for the decay $\rho \to \pi\pi$ has been taken into account by introducing an integration over the corresponding phase space. The details of this method are provided in Ref [34]. The coupling constants $g_{N^*N\omega}$ and $g_{N^*N\sigma}$ are determined by vector meson dominance hypothesis [45] and from the branching ratio of the decay of this resonance into the two pion channel [34], respectively. It should be noted that there is considerable uncertainty in the latter two coupling constants. However, the contributions of these terms to the total dilepton production amplitude are almost negligible. At the same time, since branching ratios determine only the square of the corresponding coupling constants, their signs remain uncertain in this method. Predictions from the independent calculations can, however, be used to constrain these signs [44,46,47]. Guided by the results of these studies, we have chosen the positive sign for the coupling constants for these vertices. The values of various coupling constants are given in Table II.

As in Refs. [44,45], we have used the following form factor for the N^*N vertices

$$F_j^{NN^*} = \left[\frac{(\lambda_j^{N^*})^4}{(\lambda_j^{N^*})^4 + (q_j^2 - m_j^2)^2}\right], \quad j = \pi, \rho, \omega, \sigma, \quad (14)$$

with the value of the cutoff parameter being 0.8 GeV in all the cases. It may, however, be mentioned that identical results will be obtained if one uses the form factor as given by Eq. (12) with different cutoff parameters.

C. Nucleon-nucleon-photon vertex

In the nucleonic bremsstrahlung process of dilepton production the intermediate nucleon is necessarily off-shell. The general form of the effective Lagrangian is given by

$$\mathcal{L}_{NN\gamma} = -e\bar{\Psi}\Gamma_\mu^{NN\gamma}\Psi A^\mu, \quad (15)$$

where the half-off-shell nucleon-photon vertex function Γ_μ is [48–50]

$$\Gamma_\mu^{NN\gamma} = -ie\sum_{s=\pm}(F_1^s\gamma_\mu + F_2^s\Sigma_\mu + F_3^s k_\mu)\Lambda_s. \quad (16)$$

In Eq. (16), $k^2 = (p_f - p_i)^2$ with p_f and p_i being the initial and final nucleon four momenta. $\Lambda_\pm = (\pm\not{p} + W)/W$ are the projection operators where $W = (p^2)^{1/2}$ and $\Sigma_\mu = i\sigma_{\mu\nu}k^\nu/2m_N$. The form factors $F_{1,2,3}$ are functions of k^2, W, and m_N. Factor F_3 is not independent but is constrained by the Ward-Takahashi identity [51] (i.e., by the requirement of gauge invariance)

$$F_1^\pm = \hat{e}_N + \frac{k^2}{\pm W - m_N}F_3^\pm, \quad (17)$$

where $\hat{e}_N$ is the nucleon charge in units of $|e|$.

In this work, we have adopted the procedure followed in Refs. [29,52] where one uses the on-shell form of the vertex function also for the off-shell momenta. This means, one assumes $F_1^+ = F_1^- = F_1$, $F_2^+ = F_2^- = F_2$, and $F_3^+ = F_3^- = 0$. This vertex does not, in general, satisfy gauge invariance. However, this can be achieved (see also Ref. [53]) by multiplying the external photon emission vertices by the same form factors that multiply the hadronic vertices [Eq. (6)] and by multiplying the internal photon production diagrams by the following additional factor:

$$F_{int} = 1 + \frac{m_{meson}^2 - q_1^2}{\lambda^2 - q_2^2} + \frac{m_{meson}^2 - q_2^2}{\lambda^2 - q_1^2}, \quad (18)$$

where q_1 and q_2 are the four momentum transfers at the left and right vertices, respectively. In this way, various electromagnetic form factors can be implemented for the hadrons without losing gauge invariance. Unfortunately, there are problems and ambiguities in the the selection of form factors $F_{1,2}$ (see, e.g., Ref. [54] for a detailed discussion). It has been shown already in Ref. [29] that NN bremsstrahlung contributions depend sensitively on the choice of these form factors and that cross sections calculated with no form factors are closest to the data. In our calculations, we have used the prescription [44,54] of using no form factors at the electromagnetic vertices of the nucleon term and replacing F_1 by the nucleon charge and F_2 by nucleon anomalous magnetic moment.

D. Resonance-nucleon-photon vertex

For spin-$\frac{3}{2}$ resonance-nucleon-γ vertices, the form of the vertex functions is

$$\Gamma_{RN\gamma}^{\mu\nu} = -i\frac{e}{2m_N}\left[g_1(k^2)\gamma_\lambda + \frac{g_2(k^2)}{2m_N}p_\lambda^i + \frac{g_3(k^2)}{2m_N}k_\lambda\right] \times(-k^\nu g^{\mu\lambda} + k^\mu g^{\nu\lambda})Z, \quad (19)$$

where Z is γ_5 for the even parity resonance and unity for the odd parity one. Values of the coupling constants g_1, g_2, and g_3 used in our calculations are shown in Table III. The first two are taken from [44], while the last one is taken from Ref.

TABLE III. Coupling constants for the resonance-nucleon-photon vertices used in the calculations. For $N^*(1520)$ proton couplings are given in the first line and neutron couplings in the second line.

Resonance	g_1	g_2	g_3
$\Delta(1232)$	5.416	6.612	7.0
$N^*(1520)$	3.449	5.074	1.0
	−0.307	1.862	3.0

[55]. The vertex function given by Eq. (19) fulfills gauge invariance [56] by the way of its construction.

It should be noted that the vector spinor vertices [Eqs. (9)–(12) and (19)] should in addition be contracted by an off-shell projector $\Theta_{\alpha\nu}(z)=g_{\alpha\nu}-\frac{1}{2}(1+2z)\gamma_\alpha\gamma_\nu$, where z is the off-shell parameter [44,57]. This operator describes the off-shell admixture of spin-$\frac{1}{2}$ fields [58]. The choice of the off-shell parameter z is arbitrary and it is treated as a free parameter to be determined by fitting the data. However, recently, the authors of Ref. [59] have proposed a different $\pi N\Delta$ interaction that leads to amplitudes where spin-$\frac{1}{2}$ components of the Rarita-Schwinger propagator (see in Sec. II E) drop out, thus making the off-shell parameters redundant (see, e.g., Refs. [54,59] for further details). The full implication of this prescription on observables calculated within the effective Lagrangian model will be investigated in future. In the present study we work with the couplings given by Eqs. (9)–(12) and (19).

E. Propagators

In the calculation of the amplitudes, the propagators for various mesons and nucleon resonances are required. For pion, ρ meson, and axial-vector mesons, they are given by

$$G_\pi(q)=\frac{i}{(q^2-m_\pi^2)}, \tag{20}$$

$$G_\rho^{\mu\nu}(q)=-i\left(\frac{g^{\mu\nu}-q^\mu q^\nu/q^2}{q^2-m_\rho^2}\right), \tag{21}$$

$$G_A^{\mu\nu}(q)=-i\left(\frac{g^{\mu\nu}}{q^2-m_A^2}\right). \tag{22}$$

The propagators for the ω and σ mesons are similar to those given by Eqs. (21) and (20), respectively.

The propagators for the nucleon and the spin-$\frac{3}{2}$ resonance are

$$G_N(p_i)=\frac{i(\not{p}_i+m_N)}{p_i^2-m_N^2}, \tag{23}$$

$$G_R^{\mu\nu}(p_i)=-\frac{i(\not{p}_i+m_R)}{p_i^2-[m_R-i(\Gamma_R/2)]^2}\left[g^{\mu\nu}-\frac{1}{3}\gamma^\mu\gamma^\nu-\frac{2}{3m_R^2}p_i^\mu p_i^\nu+\frac{1}{3m_R^2}(p_i^\mu\gamma^\nu-p_i^\nu\gamma^\mu)\right], \tag{24}$$

respectively. In Eq. (24), Γ_R is the total width of the resonance, which is introduced in the denominator term $(p^2-m_R^2)$ to account for the fact that the resonances are not the stable particles; they have a finite lifetime for the decay into various channels. Γ_R is a function of the center of mass momentum of the decay channel, and it is taken to be the sum of the corresponding widths for its decays to pion and ρ channels (the other decay channels are considered only implicitly by adding their branching ratios to that of the pion channel):

$$\Gamma_R=\Gamma_{R\to N\pi}+\Gamma_{R\to N\rho}. \tag{25}$$

The partial decay width $\Gamma_{R\to N\rho}$ is calculated in the same way as in Ref. [34]. This method is also identical to that used in Ref. [30]; the only difference is that while Ref. [34] uses a fully relativistic expression, that employed in Ref. [30] is its nonrelativistic counterpart. The partial width $\Gamma_{R\to N\pi}$ is taken as [30]

$$\Gamma_{R\to N\pi}(p_i)=\Gamma_0\left(\frac{k_\pi(p_i)}{k_\pi(m_R)}\right)^{2\ell+1}\left(\frac{0.25+k_\pi(m_R)^2}{0.25+k_\pi(p_i)^2}\right)^{2\ell+1}, \tag{26}$$

with

$$k_\pi(\mu)=\frac{[\{\mu^2-(m_\pi+m_N)^2\}\{\mu^2-(m_\pi-m_N)^2\}]^{1/2}}{2\mu}. \tag{27}$$

In Eq. (26), ℓ and Γ_0 are 2 and 0.095 GeV for the $N^*(1520)$ resonance, and 1 and 0.120 GeV for Δ isobar, respectively.

It should be noted that no width is included in the ρ propagator [Eq. (21)] as it corresponds to an exchange process between two nucleons where q^2 is in the spacelike region and hence ρ meson has a zero width. However, this width is finite in the ρ propagator in, e.g., $NN\to NN\rho\to NNe^+e^-$ process where the corresponding momentum is timelike.

F. Amplitudes and cross sections

After having established the effective Lagrangians, coupling constants and the form of the propagators, we can now proceed to calculate the amplitudes for various diagrams associated with the $NN\to NNe^+e^-$ reaction. These amplitudes can be written by following the well known Feynman rules [51] and can be calculated numerically. It should be stressed here that the signs of the various amplitudes are fixed, by those of the effective Lagrangians, coupling constants and the propagators as described above. These signs are not allowed to change anywhere in the calculations.

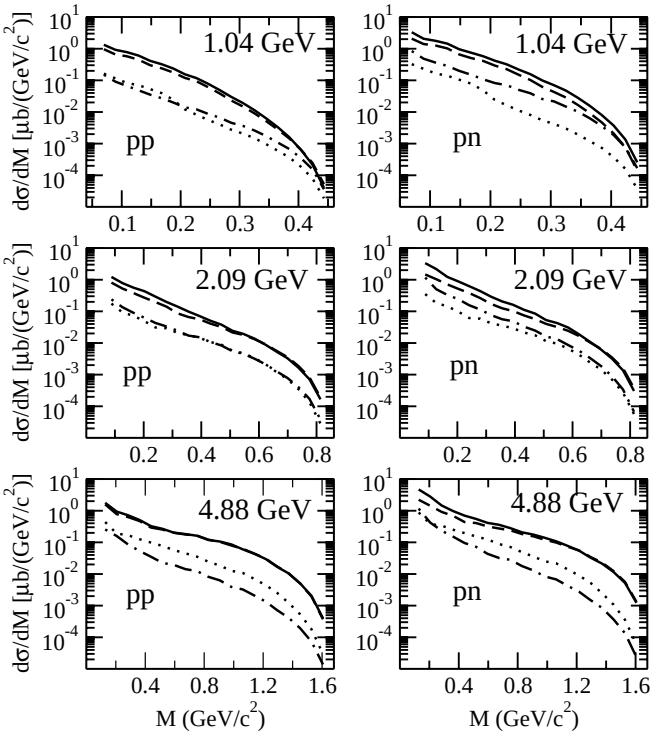

FIG. 2. Calculated invariant mass distributions for dileptons produced in proton-proton (left panel) and proton-neutron collisions (right panel) at the beam energies of 1.04 GeV, 2.09 GeV, and 4.88 GeV. The contributions of the NN bremsstrahlung (nonresonance), and the delta isobar and $N^*(1520)$ resonance states are shown by dashed-dotted, dashed, and dotted lines, respectively. Their coherent sum is shown by solid lines.

The general formula for the invariant cross section of the $N+N\rightarrow N+N+e^+e^-$ reaction is written as

$$d\sigma=\frac{m_N^4 m_e^2}{2\sqrt{[(p_1\cdot p_2)^2-m_N^4]}}\frac{1}{(2\pi)^8}\times\delta^4(P_f-P_i)|A^{fi}|^2\prod_{a=1}^{4}\frac{d^3p_a}{E_a}, \tag{28}$$

where A^{fi} represents the total amplitude, P_i and P_f represent the sum of all the momenta in the initial and final states, respectively, and p_a is the momenta of the particles in the final state. In Eq. (28) m_e represents the mass of the electron. The term $|A^{fi}|$ already includes a sum over final spin and average over initial spin degrees of freedom of all particles. More details of the evaluation of Eq. (28) are given in Appendix A.

III. RESULTS AND DISCUSSIONS

In Fig. 2, we show the invariant mass spectra for dilepton production in both pp and pn collisions at bombarding energies of 1.04 GeV, 2.09 GeV, and 4.88 GeV. It can be noted that in all the cases the dominant contribution arises from the intermediate states consisting of the Δ isobar resonance. In fact the total yields are almost equal to the contributions of the Δ amplitude alone. The pn cross sections are about a factor of 2–3 larger than those for the pp reactions even at the higher beam energy of 4.88 GeV. For beam energies of 1.04 GeV and 2.09 GeV, the contributions of the $N^*(1520)$ terms are similar to those of the NN bremsstrahlung processes for the pp collisions, while for the pn case the latter are larger than the former. However, at 4.88 GeV, the N^* channel prevails over the bremsstrahlung one in both cases. Anyway, the Δ isobar production terms are still dominant even at this high energy.

The contributions of the nucleon bremsstrahlung process (graphs involving only intermediate nucleon lines) are considerably larger in the case of pn reaction as compared to those for the pp case for all the beam energies. We do not observe the reversal of this trend at 4.88 GeV as seen in the soft-photon model calculations of Ref. [28] (where NN bremsstrahlung is larger for pp reaction as compared to that for pn one). On the other hand, if the off-shell behavior of the effective NN interaction is described by using a T matrix that includes the Δ degrees of freedom, instead of the meson exchange mechanism as employed in our model, the pp bremsstrahlung contributions turn out to be larger than those of ours at the bombarding energy of 1 GeV. Yet due to lack of calculations for the pn case, it may not be possible to make comments about the relative pp and pn bremsstrahlung contributions within this approach. In any case, the coherent sum of the Δ and bremsstrahlung terms as obtained within our model is similar to that calculated with the T matrix method.

The role of the interference effects between various terms is investigated explicitly in Fig. 3, where we compare the cross sections obtained by coherent and incoherent summations of the amplitudes corresponding to various processes shown in Fig. 2. The former are the same as those shown by solid lines in Fig. 2. It is already noted in Fig. 2 that the delta contributions are slightly larger than the total ones at the larger mass end of the spectrum for all the beam energies in both the cases. In Fig. 3, one can further see that the interference effects are noticeable towards the larger mass ends of the spectra for beam energies below 4.88 GeV in case of pp collisions. For the 4.88 GeV case these effects show up also at lower values of the invariant mass. On the other hand, they are relatively smaller for the pn case everywhere.

Contributions of various terms to the excitation function (integrated dilepton cross section) are shown in Fig. 4 for the pp (top) and pn (bottom) collisions. The total cross section at 1.04 GeV is slightly larger than that at 1.27 GeV in both the cases. However, after this it rises monotonically with the beam energy. The delta isobar terms dominate the total production yields for all the beam energies. For pp collisions, NN bremsstrahlung and $N^*(1520)$ terms are of similar magnitude except at the beam energy of 4.88 GeV where the latter term is larger than the former. However, in the pn case, the NN bremsstrahlung contributions are larger than those of the $N^*(1520)$ at lower beam energies while the two terms contribute similarly at 4.88 GeV. Furthermore, the difference in the interference effects of various terms in the two cases should also be noted. Cross sections obtained by coherent (shown by open circles) and incoherent (shown by plus

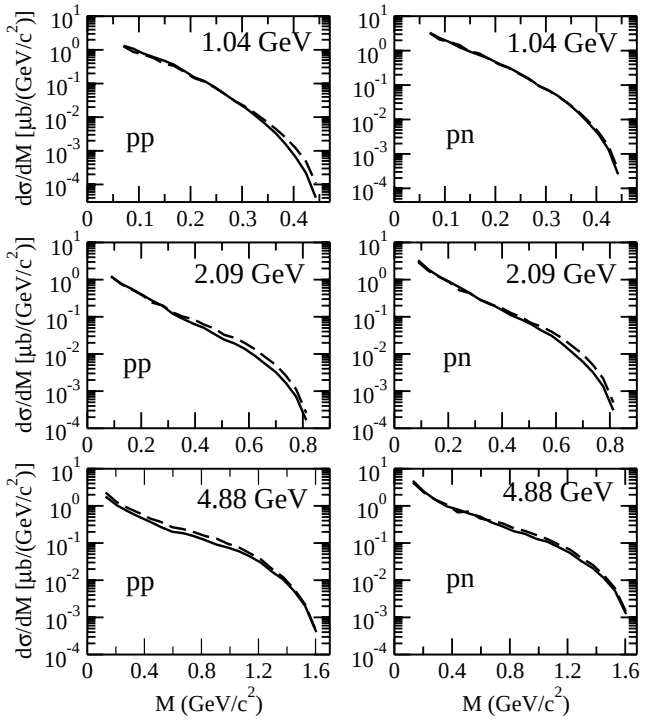

FIG. 3. Calculated invariant mass distributions for dileptons produced in proton-proton (left panel) and proton-neutron collisions (right panel) at the beam energies of 1.04 GeV, 2.09 GeV, and 4.88 GeV. Solid and dashed lines show the cross sections obtained by coherent and incoherent summations of the amplitudes of various processes shown in Fig. 2, respectively.

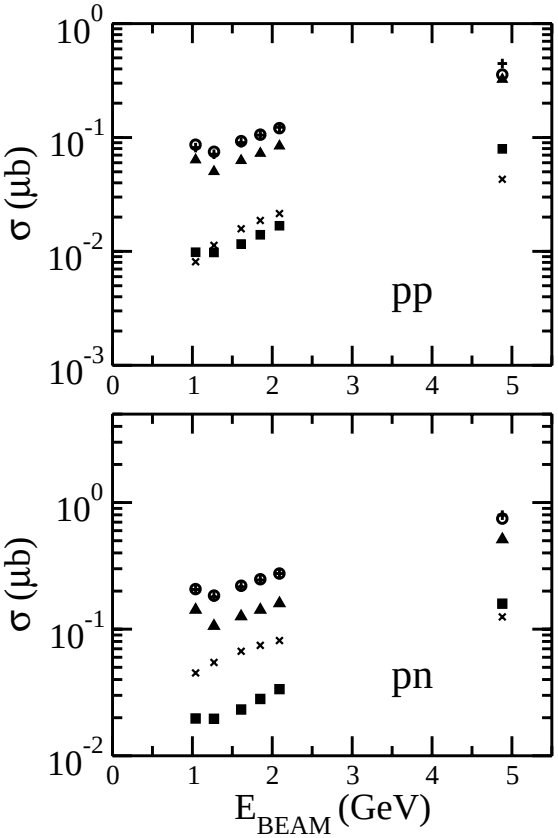

FIG. 4. Total dilepton production cross section in proton-proton (top) and proton-neutron (bottom) collisions as a function of beam energy. The nucleon, delta isobar, and $N^*(1520)$ contributions are shown by crosses, filled triangles, and solid squares, respectively. The total cross sections obtained by coherent and incoherent summations of the corresponding amplitudes are shown by open circles and plus signs, respectively.

signs) summations of the amplitudes differ very slightly for all the beam energies in case of the pn collisions and at energies smaller than 4.88 GeV for the pp case. This can be understood from the fact that the regions where the interference effects are visible in Fig. 3, contribute very little to the integrated cross sections for these cases. However, the interference effects do show up even in the total dilepton yields for pp collisions at 4.88-GeV beam energy.

The cross sections shown in Figs. 2 and 3 cannot be compared straightaway with the data of the DLS collaboration. They have to be folded with appropriate experimental filter, which is a function of the invariant mass M, transverse momentum p_T, and the rapidity in the laboratory frame (y_{lab}) of the produced dileptons. We have used the DLS acceptance filter (version 4.1) in the folding procedure. In Fig. 5, we present a comparison of the folded invariant mass spectra (which also include the final mass resolution [30]) and the data from the DLS Collaboration. We note that at beam energies of 1.04 GeV and 1.27 GeV the effective Lagrangian model calculations are able to describe the data reasonably well in the $M>0.1$ GeV region. However, at beam energies higher than 1.27 GeV, our calculations fail to reproduce the data, being lower than them by factors ranging from 2–20. Clearly, with increasing beam energy, other dilepton sources become important; these include Dalitz decays of hadrons (π^0, η, and ω) [23,30,31], direct decay of the ω and ρ^0 mesons to dileptons, processes leading to multihadronic final states [28], and two pion annihilation [60]. Nevertheless, it is encouraging that the present effective Lagrangian model is able to account for the dilepton yields in pp collisions at beam energies around 1.0 GeV. Therefore, this theory could be useful in making predictions for the dilepton spectra to be measured by the HADES spectrometer at GSI, for beam energies in this region.

In order to study the role of other dilepton production processes not considered in the present effective Lagrangian model, we have included the contributions of the Dalitz decays: $\pi^0 \to \gamma e^+ e^-$ and $\eta \to \gamma e^+ e^-$, and the direct decays $\rho^0 \to e^+ e^-$ and $\omega \to e^+ e^-$. The details of these calculations are described in Ref. [30] and important relevant formulas are listed in Appendix B. The cross sections of these processes were incoherently summed to those of the total mass differential cross sections (solid lines in Fig. 5) of the ELM. The results are shown in Fig. 6 together with the DLS data. At the beam energies of 1.04 GeV and 1.27 GeV, we have shown explicitly only the contributions of π^0 and π^0 and η decay processes, respectively, together with the ELM results as cross sections for the other decay channels are insignificant here. At incident energies of 1.61 GeV and 1.85 GeV we show, in addition, the contributions of ρ^0 direct decay also; the ω direct decay is insignificant at these energies. How-

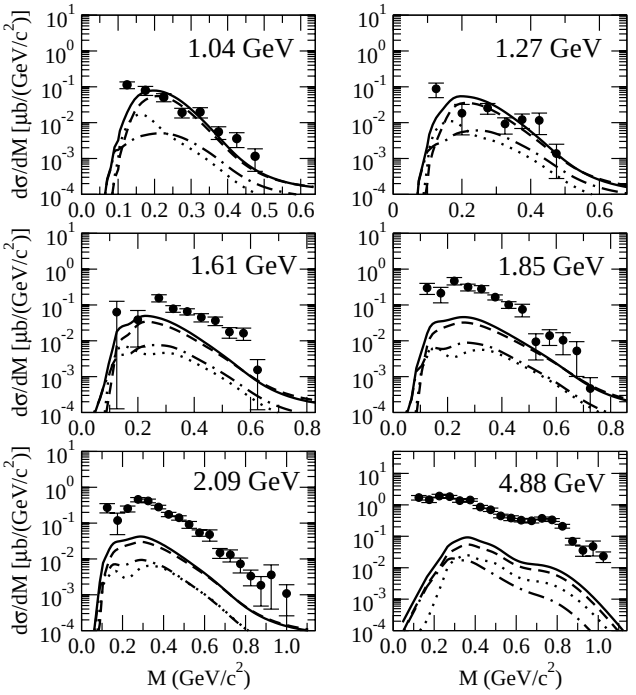

FIG. 5. Comparison of the effective Lagrangian model results for the invariant mass spectra of dileptons produced in proton-proton collisions, folded with the experimental filter, with the data of the DLS Collaboration [38] at the beam energies of 1.04 GeV, 1.27 GeV, 1.61 GeV, 1.85 GeV, 2.09 GeV, and 4.88 GeV. The curves have the same meaning as in Fig. 2. The solid circles show the experimental data.

ever, at 2.09 GeV and 4.88 GeV, contributions of all the decay channels as mentioned above are shown explicitly.

It is clear that now the data can be described reasonably well for all the beam energies. This comparison suggests that the lowest points in the mass distributions of the dilepton stem from the π^0 Dalitz decay. The η Dalitz decay is important at the intermediate masses for beam energies between 1.61 GeV and 4.88 GeV, while the ρ^0 and ω direct decay processes are important at higher mass ends of the spectra for these beam energies. In addition to these processes, the multihadron final state bremsstrahlung mechanism could also contribute significantly in the low mass region at the beam energy of 4.88 GeV [28]. We would like to mention that although several processes are included in our results shown in Fig. 6, the double counting problem is unlikely to be present there. The Dalitz decay and the direct decay processes of dilepton production are excluded from the effective Lagrangian treatment. Furthermore, we have not considered the processes such as $NN \to NR \to NN\rho^0 \to NNe^+e^-$ (termed as the subthreshold resonance production). Therefore, problems of double counting in the vector meson direct decay contributions as suggested in Ref. [61] are not present in our calculations.

IV. SUMMARY AND CONCLUSIONS

We investigated the dilepton production in the nucleon-nucleon collisions at beam energies in the range of 1–5 GeV within an effective Lagrangian model, which in proven to describe well the pion and kaon production in NN collisions. Most of the parameters of this model are fixed by fitting to the elastic NN T matrix; this restricts the freedom of varying the parameters of the model to provide a fit to the data. Along with the NN bremsstrahlung process, the model also includes the excitation, propagation and radiative decay of the $\Delta(1232)$ and $N^*(1520)$ intermediate nucleon resonant states. The coupling constants at vertices involving resonances have been determined from the experimental branching ratios of their decay into various relevant channels. The interference terms among various amplitudes are included in the total T matrix.

The reaction proceeds predominantly via excitation of the Δ intermediate state in the entire beam energy range considered in this work. The contributions of the $N^*(1520)$ terms are relatively small. The NN bremsstrahlung contributions are also weak in comparison to those of the delta isobar except for the higher mass region of the invariant mass spectra at the beam energy of 1.04 GeV. In this region of these spectra considerable interference between various terms is also visible. For the case of pp collisions, the NN bremsstrahlung and $N^*(1520)$ contributions are similar in magnitude at lower beam energies. However, for the pn case, the former is larger than the latter at these energies. On the other hand, for the beam energies of 4.88 GeV, the $N^*(1520)$ terms are larger than those of the bremsstrahlung in both the cases. A key result of our study is that the pn bremsstrahlung is stronger than the pp one even at the beam energy of 4.88 GeV.

At the lower beam energies (1.04 GeV and 1.27 GeV), the effective Lagrangian model calculations are able to explain the data of the DLS Collaboration for the invariant mass distribution of dilepton emitted in pp collisions except for the lowest mass point. This is encouraging in the context of the analysis of the new experimental data on the dilepton production expected shortly from the HADES collaboration at GSI, Darmstadt.

However, at higher beam energies (1.61 GeV, 1.85 GeV, 2.09 GeV, and 4.88 GeV), the effective Lagrangian model underpredicts the DLS data. This indicates that with increasing energy, other dilepton production sources become important. To stress this point further, we incoherently summed the π^0 and η Dalitz decay and the ρ^0 and ω direct decay contributions to the cross sections of the ELM. With this procedure, it is possible to provide a good description of the DLS data on the invariant mass distribution at all the beam energies. This also removes the discrepancy observed between the effective Lagrangian model calculations and the DLS invariant mass distribution data for the lowest mass point at the beam energies of 1.04 GeV and 1.27 GeV.

Our study has clarified the role of the Δ and $N^*(1520)$ intermediate baryonic resonance states in the dilepton production in the NN collisions. The interference effects of various terms are visible towards the large invariant mass ends of the spectra for proton-proton collisions. However, the DLS experimental filter effectively cuts off this mass region. Therefore, these effects do not show up when calculations-

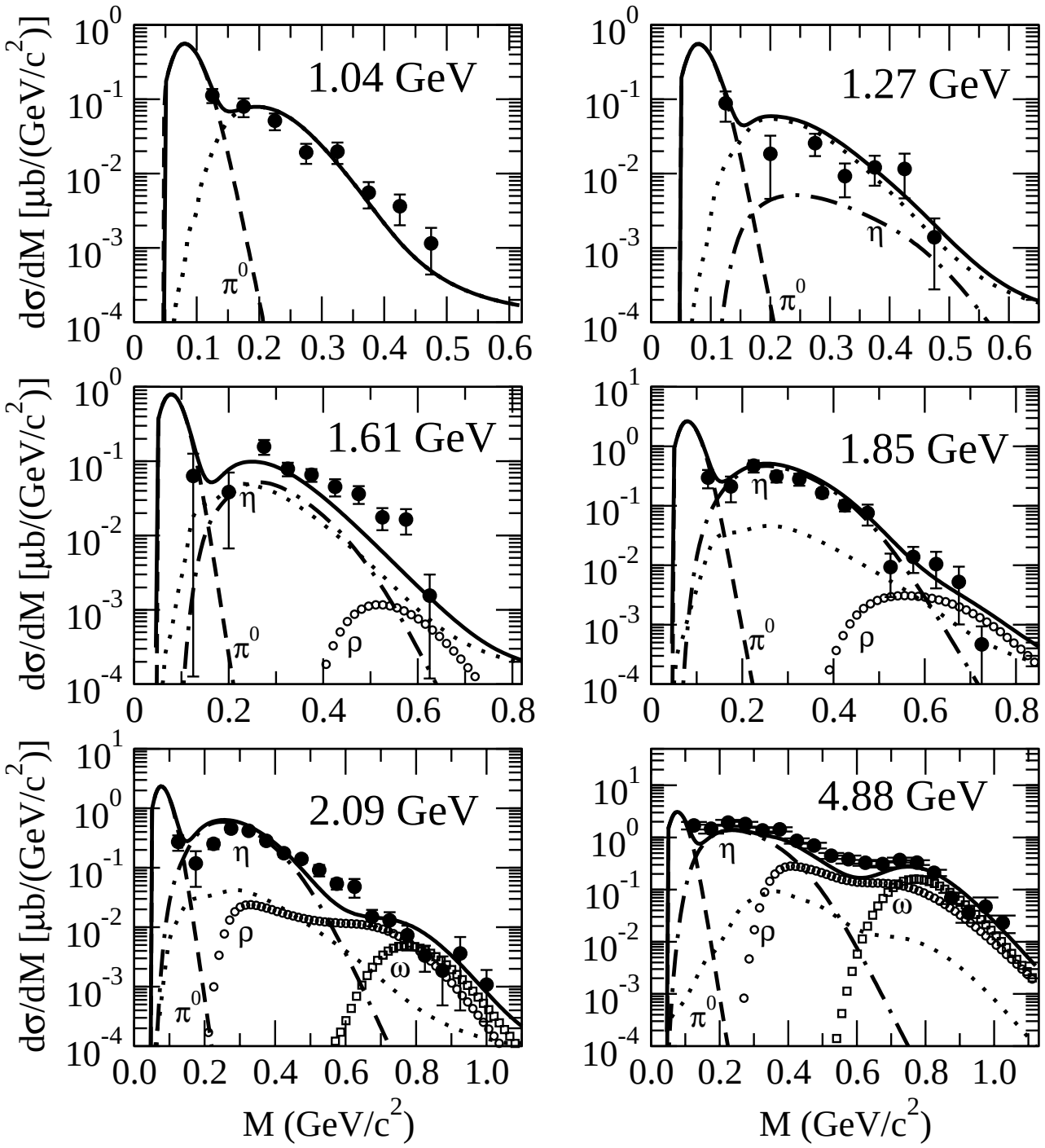

FIG. 6. The calculated dilepton invariant mass spectra for proton-proton collisions in the beam energy range of 1.04–4.88 GeV in comparison to the DLS data [38]. The effective Lagrangian model results are shown by the dotted lines (the same as those shown by full lines in Fig. 4). The contributions of π^0, η Dalitz decay, and ρ^0 and ω direct decay processes are shown by dashed, dashed-dotted, open circles, and open squares, respectively. The incoherent sum of these cross sections with those of the effective Lagrangian model is shown by the solid line. Solid circles represent the experimental data.

are compared with the data. This may imply that an incoherent combination of resonance and decay contributions is sufficient to explain the DLS data. However, with improved quality of the data this impression could change. Therefore, precise data, where also the hadrons in the final channel are detected, would be welcome. This would put constraint on the models calculating the role of various mechanisms in the dilepton production in nucleon-nucleon collisions. The present effective Lagrangian approach should be improved by including the amplitudes for the decay processes also so that they can be summed coherently with the amplitudes of the other channels already included.

ACKNOWLEDGMENTS

This work was supported by the Foschungszentrum Jülich. One of the authors (R.S.) would like to thank Elena Bratkovskaya for several useful and clarifying discussions about the work presented in Refs. [30,31] and help in implementing the filter program of the DLS Collaboration.

APPENDIX A: SOME DETAILS OF THE PHASE SPACE AND THE AMPLITUDE

In this appendix we give additional details of calculations of the four-body phase space factor and amplitude A^{fi}.

The kinematical situation for calculating the differential cross section [Eq. (28)] is illustrated in Fig. 7 where $\mathbf{p}_1$ and $\mathbf{p}_2$ depict the initial momenta of two nucleons while $\mathbf{p}_3$ and $\mathbf{p}_4$ their final momenta. The momenta of e^+ and e^- are shown by $\mathbf{p}_+$ and $\mathbf{p}_-$, respectively. $\mathbf{P}$ represents half of the total center of mass (c.m.) dilepton momentum. The differential cross section can be written as [26]

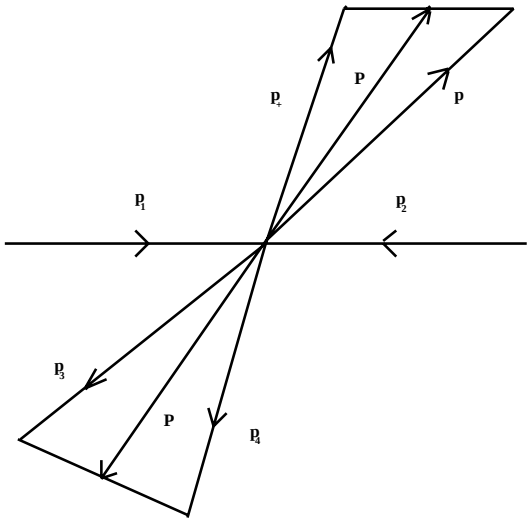

FIG. 7. Illustration of the kinematical situation for e^+e^- pair production in NN collisions. $\mathbf{p}_1$ and $\mathbf{p}_2$ are the initial nucleon momenta in the c.m. system while $\mathbf{p}_3$ and $\mathbf{p}_4$ are the same for the final nucleons. $\mathbf{P}$ is half of the total dilepton momentum.

$$\frac{d\sigma}{dM d\Omega_P dP d\Omega_{Q_L} d\Omega_{Q_N}} = \frac{4m_N^4 m_e^2 P^2 Q_L^2 Q_N^2}{[E_{l+}Q_L - E_{l-}|P|\cos\theta_1][(E_3+E_4)Q_N + (E_3-E_4)|P|\cos\theta_2]} \frac{M}{E_{l+}E_p|P_p|(2\pi)^8}|A^{fi}|^2, \tag{A1}$$

where $\mathbf{Q}_L = \mathbf{p}_- - \mathbf{P}$ and $\mathbf{Q}_N = \mathbf{p}_3 + \mathbf{P}$. θ_1 and θ_2 are angles between $\mathbf{P}$ and $\mathbf{Q}_L$, and $\mathbf{P}$ and $\mathbf{Q}_N$, respectively. In Eq. (A1), we have defined $E_{l+} = E_+ + E_-$ and $E_{l-} = E_+ - E_-$, where E_+ and E_- are energies of e^+ and e^-, respectively. E_p and $|P_p|$ are the energy and momentum of the projectile nucleon in the c.m. system. The invariant mass of the dilepton is given by $M^2 = (p_+ + p_-)^2$. Integrations over the residual degrees of freedom in the differential cross section [Eq. (A1)] are carried out by using the Monte Carlo techniques.

A total of 90 diagrams [42 for NN bremsstrahlung, and 16 and 32 involving Δ and $N^*(1520)$ intermediate states, respectively] contribute to amplitude A^{fi}. Due to their large number, it is hard to calculate them by usual trace techniques. Instead we follow the procedure given below.

We first note that amplitude corresponding to each individual diagram can be split into a hadronic part and a leptonic part as

$$A^{fi} \sim h_\mu^{fi} \frac{g^{\mu\nu}}{k^2} l_\nu^{fi}. \tag{A2}$$

For example, for the diagram of type (a) of Fig. 1, involving pion exchange and the nucleon intermediate state (NN bremsstrahlung), we have

$$h_\mu^{fi} = -i\left(\frac{g_{NN\pi}}{2m_N}\right)^2 \frac{1}{q^2 - m_\pi^2} \bar{u}(p_4,s_4)\gamma_5 \not{q} u(p_2,s_2)\bar{u}(p_3,s_3) \times \Gamma_\mu^{NN\gamma} \frac{(\not{p}_i + m_N)}{p_i^2 - m_N^2}\gamma_5 \not{q} u(p_1,s_1) f_{iso}, \tag{A3}$$

$$l_\nu^{fi} = e\bar{u}(p_+,s_+)\hat{e}\gamma_\nu u(p_-,s_-), \tag{A4}$$

where $u(p_i,s_i)$ are free Dirac spinors with four momentum p_i and spin s_i, and $\Gamma_\mu^{NN\gamma}$ is the same as defined in Eq. (16). f_{iso} is the isospin factor, which for each graph is obtained from the separate treatment of the isospin parts. In Eq. (A4) $\hat{e}$ is $\frac{1}{2}(1+\tau_3)$. Similar expressions for the amplitudes corresponding to all the graphs can be written in a straight forward way by using the Lagrangians and the propagators given in the main text.

The summation over spins of the modulus square of the leptonic part gives

$$L_{\mu\nu} = \sum_{spins} l_\mu^{fi\dagger} l_\nu^{fi} = \frac{e^4}{4m_e^2}[-2g_{\mu\nu}M^2 + 4(p_{+\mu}p_{-\nu} + p_{+\nu}p_{-\mu})]. \tag{A5}$$

In the evaluation of the hadronic part of the amplitudes we encounter terms of the form

$$T_{\mu}^{NI}=\overline{u}(p_3,s_3)\gamma_{\mu}\frac{p_{i\nu}\gamma^{\nu}+m_j}{(p_i^2-m_j^2)}\Gamma_{eff}^{NI}u(p_1,s_1), \qquad \text{(A6)}$$

where Γ_{eff}^{NI} is a linear combination of 16 4×4 Dirac matrices $(1,\ \gamma_{\mu},\sigma_{\mu\nu},\gamma_5,\gamma_5\gamma_{\mu})$ and m_j is the mass of either nucleon or the resonance. In the latter case, it also includes the resonance width as shown in Eq. (24). Further calculations of such terms are carried out by using the manipulator package REDUCE. The matrix elements so calculated are summed together as complex numbers. The result still depends on the initial and final spins of the nucleons. The modulus square of this sum is then averaged over the initial spins and summed over the final spin states. This leads to $|A^{fi}|^2$. By this procedure a large number of matrix manipulations are avoided.

APPENDIX B: CALCULATIONS OF DALITZ DECAYS AND DIRECT DECAY OF MESONS

In this appendix, we describe briefly calculations of Dalitz decays $\eta\rightarrow\gamma e^+e^-$ and $\pi^0\rightarrow\gamma e^+e^-$, and direct decays $V\rightarrow e^+e^-$ $(V=\rho$ and $\omega)$. More details can be found in Ref. [30].

The calculation of the process $pp\rightarrow XM\rightarrow X\gamma e^+e^-$ proceeds in two steps. First the meson M (η and π) is produced in the pp collisions and then the Dalitz decay $M\rightarrow\gamma e^+e^-$ is considered. In the procedure of Ref. [30], the parametrization of Refs. [3,14,62] are used to calculate the M production cross sections. The η Dalitz decay to γe^+e^- is given by (see also Ref. [63])

$$\frac{d\Gamma_{\eta\rightarrow\gamma e^+e^-}}{dM}=\frac{4\alpha}{3\pi}\frac{\Gamma_{\eta\rightarrow2\gamma}}{M}\left(1-\frac{4m_e^2}{M^2}\right)^{1/2}\left(1+2\frac{m_e^2}{M^2}\right)^{1/2}\times\left(1-\frac{M^2}{m_{\eta}^2}\right)^{1/2}|F_{\eta\rightarrow\gamma e^+e^-}(M)|^2, \qquad \text{(B1)}$$

where the form factor is parametrized as

$$F_{\eta\rightarrow\gamma e^+e^-}(M)=\left(1-\frac{M^2}{\Lambda_{\eta}^2}\right)^{-1}. \qquad \text{(B2)}$$

The value of parameter Λ_{η} is 0.72 GeV. In Eq. (B1), α represents the fine structure constant, and $\Gamma_{\eta\rightarrow2\gamma}$ is the partial width for the $\eta\rightarrow2\gamma$ decay whose value is adopted from the Particle Data Group compilation [64].

The Dalitz decay $\pi^0\rightarrow\gamma e^+e^-$ is calculated in the same way using the following form factor:

$$F_{\pi^0\rightarrow\gamma e^+e^-}(M)=(1+B_{\pi^0}M^2), \qquad \text{(B3)}$$

with $B_{\pi^0}=5.5\ \text{GeV}^{-2}$.

Similarly, calculations of the direct decay of the ρ and ω mesons proceeds in two steps; the production of these meson in pp collisions is calculated in the first step and their decay to dilepton in the second,

$$\frac{d\sigma(M)}{dM}_{NN\rightarrow VNN\rightarrow e^+e^-NN}=\frac{d\sigma(M)}{dM}_{NN\rightarrow VNN}\frac{\Gamma_{V\rightarrow e^+e^-}(M)}{\Gamma_{tot}^{V}(M)}. \qquad \text{(B4)}$$

The calculation of the first term on the right hand side is described in detail in Ref. [30] and will not be repeated here. The decay width $\Gamma_{V\rightarrow e^+e^-}(M)$ is given by

$$\Gamma_{V\rightarrow e^+e^-}(M)=C_V\frac{m_V^4}{M^3}, \qquad \text{(B5)}$$

where $C_V=8.8\times10^{-6}$ and 0.767×10^{-6} for $V=\rho$ and ω, respectively. The total vector meson decay width Γ_{tot}^{V} is defined in the same way as in Ref. [30]. We refer to Ref. [61] for a more recent description of these calculations.

[1] C. Gale and J. Kapusta, Phys. Rev. C **35**, 2107 (1987).
[2] L.H. Xia, C.M. Ko, L. Xiang, and J.R. Wu, Nucl. Phys. **A485**, 721 (1988).
[3] Gy. Wolf, G. Batko, W. Cassing, U. Mosel, K. Niita, and M. Schäfer, Nucl. Phys. **A517**, 615 (1990).
[4] U. Mosel, Annu. Rev. Nucl. Part. Sci. **41**, 29 (1991).
[5] G.E. Brown and M. Rho, Phys. Rev. Lett. **66**, 2720 (1991).
[6] T. Hatsuda and S. Lee, Phys. Rev. C **46**, R34 (1992).
[7] G. Chanfray and P. Schuck, Nucl. Phys. **A545**, 271c (1992).
[8] M. Herrmann, B. Friman, and W. Nörenberg, Nucl. Phys. **A560**, 411 (1993).
[9] M. Asakawa and C.M. Ko, Phys. Rev. C **48**, R526 (1993).
[10] C.M. Shakin and W.D. Sun, Phys. Rev. C **49**, 1185 (1994).
[11] F. Klingl and W. Weise, Nucl. Phys. **A606**, 329 (1996); F. Klingl, N. Kaiser, and W. Weise, *ibid.* **A624**, 527 (1997).
[12] R. Rapp, G. Chanfray, and J. Wambach, Nucl. Phys. **A617**, 496 (1997).
[13] S. Leupold, W. Peters, and U. Mosel, Nucl. Phys. **A628**, 311 (1998).
[14] Gy. Wolf, W. Cassing, and U. Mosel, Nucl. Phys. **A552**, 549 (1993).
[15] G. Agakichiev *et al.*, Phys. Rev. Lett. **75**, 1272 (1995); Th. Ullrich *et al.*, Nucl. Phys. **A610**, 317c (1996).
[16] M. Masera, Nucl. Phys. **A590**, 93c (1995).
[17] G.Q. Li, C.M. Ko, and G.E. Brown, Phys. Rev. Lett. **75**, 4007 (1995).
[18] C.M. Ko, G.Q. Li, G.E. Brown, and H. Sorge, Nucl. Phys. **A610**, 342c (1996).
[19] W. Cassing, W. Ehehalt, and C.M. Ko, Phys. Lett. B **363**, 35 (1995); W. Cassing, W. Ehehalt, and I. Kralik, *ibid.* **377**, 5 (1996).

[20] E.L. Bratkovskaya and W. Cassing, Nucl. Phys. **A619**, 413 (1997).
[21] W. Cassing, E.L. Bratkovkaya, R. Rapp, and J. Wambach, Phys. Rev. C **57**, 916 (1998).
[22] E.L. Bratkovkaya, W. Cassing, R. Rapp, and J. Wambach, Nucl. Phys. **A634**, 168 (1998).
[23] C. Ernst, S.A. Bass, M. Belkasem, H. Stöcker, and W. Greiner, Phys. Rev. C **58**, 447 (1998).
[24] E.L. Bratkovkaya and C.M. Ko, Phys. Lett. B **445**, 265 (1999).
[25] R.J. Porter *et al.*, Phys. Rev. Lett. **79**, 1229 (1997).
[26] M. Schäfer, T.S. Biro, W. Cassing, and U. Mosel, Phys. Lett. B **221**, 1 (1989).
[27] C. Gale and J. Kapusta, Phys. Rev. C **40**, 2397 (1989).
[28] K. Haglin and C. Gale, Phys. Rev. C **49**, 401 (1994).
[29] M. Schäfer, H.C. Dönges, A. Engel, and U. Mosel, Nucl. Phys. **A575**, 429 (1994).
[30] E.L. Bratkovskaya, W. Cassing, M. Effenberger, and U. Mosel, Nucl. Phys. **A653**, 301 (1999).
[31] E.L. Bratkovskaya, W. Cassing, and U. Mosel, Nucl. Phys. **A686**, 568 (2001).
[32] A. Engel, R. Shyam, U. Mosel, and A.K. Dutt-Majumder, Nucl. Phys. **A603**, 387 (1996).
[33] R. Shyam and U. Mosel, Phys. Lett. B **426**, 1 (1998).
[34] R. Shyam, Phys. Rev. C **60**, 055213 (1999); R. Shyam, G. Penner, and U. Mosel, *ibid.* **63**, 022202(R) (2001).
[35] F. de Jong and U. Mosel, Phys. Lett. B **379**, 45 (1996).
[36] K.L. Haglin, Ann. Phys. (N.Y.) **212**, 84 (1991).
[37] A.I. Titov, B. Kämpfer, and E.L. Bratkovskaya, Phys. Rev. C **51**, 227 (1995).
[38] W.K. Wilson *et al.*, Phys. Rev. C **57**, 1865 (1998).
[39] T. Ericson and W. Weise, *Pions and Nuclei* (Clarendon, Oxford, 1988).
[40] G. Penner, Ph.D. thesis (in English), Universität Giessen, 2002, available at the URL http://theorie.physik.uni-giessen.de
[41] J. D. Bjorken and S. D. Drell, *Relativistic Quantum Mechanics* (McGraw-Hill, New York, 1964).
[42] J.W. Durso, G.E. Brown, and M. Saarela, Nucl. Phys. **A430**, 653 (1984).
[43] C. Song, C.M. Ko, and C. Gale, Phys. Rev. C **50**, R1827 (1994).
[44] T. Feuster and U. Mosel, Nucl. Phys. **A612**, 375 (1997); Phys. Rev. C **58**, 457 (1998); **59**, 460 (1999).
[45] M. Post and U. Mosel, Nucl. Phys. **A688**, 808 (2001).
[46] D.M. Manley and E.M. Saleski, Phys. Rev. D **45**, 4002 (1992).
[47] S. Capstick and W. Roberts, Phys. Rev. D **49**, 4570 (1994).
[48] A.Yu. Korchin and O. Scholten, Nucl. Phys. **A581**, 493 (1995).
[49] H.W.L. Naus and J.H. Koch, Phys. Rev. C **36**, 2459 (1987).
[50] P.C. Tiemeijer and J.A. Tjon, Phys. Rev. C **42**, 599 (1990).
[51] C. Itzykson and J. B. Zuber, *Quantum Field Theory* (McGraw-Hill, New York, 1964).
[52] K. Haglin, J. Kapusta, and C. Gale, Phys. Lett. B **224**, 433 (1989).
[53] I.S. Towner, Phys. Rep. **155**, 263 (1987).
[54] G. Penner and U. Mosel, Phys. Rev. C **66**, 055211 (2002); **66**, 055212 (2002).
[55] G. Penner, diploma thesis, University of Giessen, 1997.
[56] S. Nozawa, B. Blankleider, and T.-S.H. Lee, Nucl. Phys. **A513**, 459 (1990); S. Nozawa and T.-S.H. Lee, *ibid.* **A513**, 511 (1990).
[57] M. Benmerrouche, N.C. Mukhopadhyay, and J.F. Zhang, Phys. Rev. D **51**, 3237 (1995).
[58] M. Benmerrouche, R.M. Davidson, and N.C. Mukhopadhyay, Phys. Rev. C **39**, 2339 (1989).
[59] V. Pascalutsa, Phys. Rev. D **58**, 096992 (1998); V. Pascalutsa and R. Timmermans, Phys. Rev. C **60**, 042201(R) (1999).
[60] J. Kapusta and P. Lichard, Phys. Rev. C **40**, R1574 (1989).
[61] Amand Faessler, Christian Fuchs, Mikhail Krivoruchenko, and Boris Martemyanov, nucl-th/0010056.
[62] T. Vetter, A. Engel, T. Biro, and U. Mosel, Phys. Lett. B **263**, 153 (1991).
[63] L.G. Landsberg, Phys. Rep. **128**, 301 (1985).
[64] Particle Data Group, K. Hagiwara *et al.*, Phys. Rev. D **66**, 010001 (2002).